[Journal of the Faculty of Science, Hokkaido University, Ser. VII (Geophysics), Vol. VI, No. 2, 1980]

Sedimentation by Turbidity Currents

Kazuhisa CHIKITA

(Received Oct. 15, 1979)

Abstract

Sedimentation by turbidity currents is studied through both surveys in the field and laboratory experiment, and the close relations between the flowing mechanism and the grain-size distributions of the sediments are found out.

(1) Surveys in the field were performed in the Katsurazawa Reservoir. Measurements on sediment discharge of the influent rivers were made during the snow-melting period of April 3–29, 1977 and March 29, 1978, and as a result, the conditions of occurrence and the behaviors in the reservoir were enlightened with respect to turbidity currents. The results are as follows: a) The sediment concentrations more than 10,000 mg/l of river water flowing into the reservoir could last about 18 hours from April 15 to April 16, and the observed peak concentration reached 11,900 mg/l. b) The bottom layer of the reservoir turned so turbid as snow melting progressed. c) The difference of sediment concentration rather than water temperature have a considerable effect on that of water density between river water and reservoir water for the snow-melting period.

These indicate lasting occurrence of turbidity currents and the fact that turbidity currents can be divided into three types of overflows, interflows and underflows.

(2) Sedimentation by turbidity currents is investigated more minutely through the laboratory experiment with a flume.

The grain-size distributions of bottom sediments deposited in a flume were plotted on log-probability paper, and velocity and water concentration of flows were measured at some given points in a flume. The results are indicated that the sediments deposited in mixing zone and, as the case may be, at near plunging point can be divided into three subpopulations, i.e. traction, saltation and suspension populations, and those in turbidity currents, into four subpopulations, i.e. traction, saltation, suspension and "autosuspension" populations.

(3) Experimental results are applied to the field study from a viewpoint of grain-size distributions of bottom sediments in log-probability plots.

The sediments of Katsurazawa Reservoir also have grain-size distributions with two or three break points on log-probability paper, and the results for the break points, through establishment of flowing mechanism of turbidity currents *in situ*, represent a good agreement with the experimental ones, which shows that the reservoir sediments can be classified into four subpopulations, i.e. traction, saltation, suspension and "autosuspension" populations at near plunging point, and into three subpopulations, i.e. traction, saltation and suspension populations in the far downstream.

1. Introduction

As regards unsteady turbidity flows having the sedimentary process, the sedimentary mechanism has been studied chiefly in river flows through many laboratory experiments of open channel, concerned with the forms of a mobile bed. Nevertheless, it has been so difficult to precisely predict the sedimentary process of transported solid particles solely from the knowledge of hydraulics of flows, especially the boundary layers, which can be attributed to the complicated interaction of the suspended sediments with surrounding fluid, bed materials or themselves, close to the bed.

Turbidity currents can be a sedimentary mechanism of great importance in both oceanosphere and hydrosphere, and has ever been studied by many investigators from the sedimentological viewpoint[1)-7)] and from the hydraulic one[8)-13)].

In hydrosphere, the interesting informations on turbidity currents have once been given by comprehensive survey in the reservoir, Lake Mead[14)]. And in oceanosphere, a spectacular example has been provided by the shock of the Grand Banks earthquake of 1929, which brought about a series of delayed breaks of several submarine cables possibly through a submarine slumping and resulting turbidity current[15)].

But in general, turbidity currents may occur very catastrophically, which has ever made it very difficult to predict their occurrence and come at a true knowledge of the flows. In case of turbidity currents under sedimentation, not only the flowing mechanism but some systematic relation of it with the sediments on the bed have been little enlightened by experimental works, much less field works.

Turbidity currents by which the writer has investigated sedimentation in Katsurazawa Reservoir can be, in a type of motion, similar to those in Lake Mead[7)].

In spring runoffs and rainfall runoffs, river water more than usual will flow into a reservoir and mix with the reservoir water over a stretch downstream from the inflow point. The stretch in the head of reservoir is "mixing zone", where the most downstream point is called "critical point", "plunge point" or "plunging point". Inflow waters passing through plunging point will then turn into density currents with a flow type in accordance with the density difference between river water and reservoir water. Bulk density of water depends on the amount of suspended and dissolved solids in water and water temperature, and in case of the chief dependence of the density difference on

the amount of suspended sediments, the density currents can be considered particularly as "turbidity currents". Therefore, according to inflow of turbid river water with bulk density, higher or lower than or equal to that of the upper-layer water of reservoir, turbidity currents can be divided into three types of overflows, interflows and underflows[16]. But such turbidity currents as overflows will be rarely observed *in situ*, and otherwise density overflows, e.g. sediment plumes, frequently, which may develop on the basis of the temperature difference between inflow water and receiving water.

The writer has made a laboratory experiment and some observations of Katsurazawa Reservoir with respect to turbidity currents, and has studied sedimentation by the flows from some remarks on grain-size distributions of bottom sediments.

2. Occurrence of turbidity currents and its condition

In the previous paper[7], it was shown, on the basis of a theoretical treatment, that turbidity currents could occur during the snow-melting period every year. In order to verify this expectation, causal relation in sedimentological regime between influent river and reservoir during the period of snow-melting should be first enlightened.

The writer made observations in Katsurazawa Reservoir on sediment discharge of the influent rivers and the response of the reservoir to it during the period April 3–29, 1977 and on March 29, 1978.

2.1 Sediment discharge in spring runoff

Observations on sediment discharge in spring runoff were made by means of sampling inflow waters from the bridges across the principal arms of Katsurazawa Reservoir (Fig. 1). The bridges of B to F in Fig. 1 are the sampling points of river waters. Sampling was made chiefly at the E point over the Old Ikushunbetsu and at the F point over the Ikushunbetsu River.

Katsurazawa Reservoir has lower water level during the period of the last decade of March to the first decade of April every year (Fig. 28) and as a result, the observations were made at E for 3–16 and F for 17–29 April. Since there accumulates little remainder of the reservoir sediments in the upstream from each of the sampling points, it is seen the sediment discharge almost resulted from sediment yield induced by snow melting.

Fig. 2 and Table 1 indicate the results of observations. Discharge of river water was calculated on the basis of the data of water level and inflow and

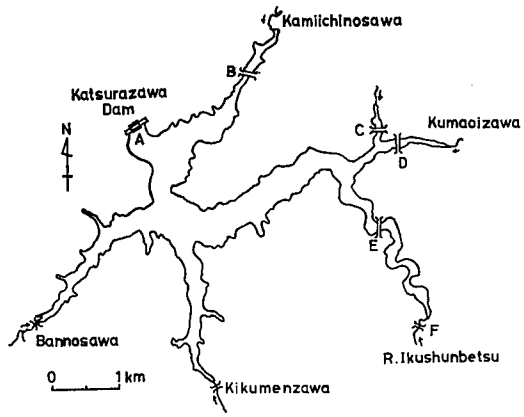

Fig. 1 Sampling points of river waters.

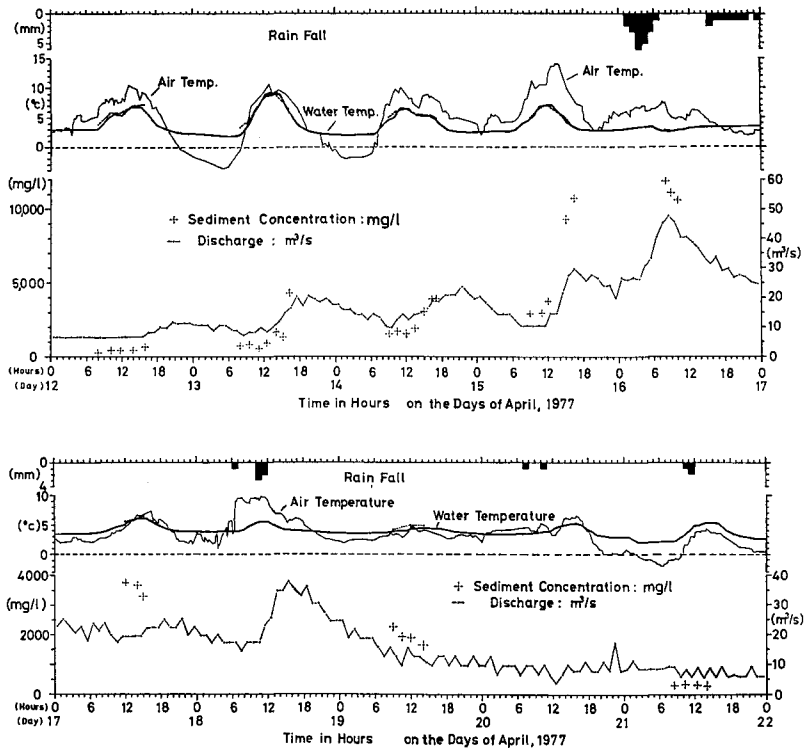

Fig. 2 Observational results on sediment discharge at the points of E (upper) and F (lower).

Table 1 Data on sediment discharge at the time of sampling on each of the points of B to F.

Sampling Point	Day	Time	Water Temp. (°C)	Sediment Conc. (mg/l)	Density (g/cm³)
E	8	7:21	3.0	163.0	1.000094
		9:05	4.1	243.5	1.000152
		10:18	5.5	182.5	1.000096
		11:48	7.5	401.5	1.000155
		13:23	8.0	282.5	1.000053
		14:46	7.5	359.0	1.000129
		16:20	6.0	920.5	1.000543
E	9	7:08	2.8	395.0	1.000235
		8:43	4.0	420.5	1.000262
		10:14	5.6	397.0	1.000227
		11:39	6.8	413.0	1.000196
		13:14	7.7	687.0	1.000323
		14:38	7.3	626.0	1.000306
		15:56	6.2	824.0	1.000476
E	10	11:10	4.0	921.5	1.000575
F		12:23	4.3	393.0	1.000245
E		12:37	4.2	813.0	1.000507
D		12:50	1.7	109.0	1.000025
B		13:15	3.9	1083	1.000676
E	11	7:16	2.4	642.5	1.000383
		8:45	3.1	784.0	1.000483
		10:50	4.0	547.5	1.000342
		12:41	5.0	860.5	1.000529
		14:41	5.9	606.0	1.000349
		16:10	5.6	524.5	1.000307
E	12	8:00	3.8	253.0	1.000158
		10:15	5.9	412.0	1.000228
		11:45	5.8	412.5	1.000232
		13:57	7.1	490.5	1.000231
		15:53	7.3	684.0	1.000342
E	13	8:02	3.5	775.5	1.000482
		9:26	4.6	830.0	1.000515
		11:08	7.1	570.5	1.000281
		12:27	8.9	972.5	1.000423
		14:02	9.0	1704	1.000872
		15:10	8.0	1389	1.000743
		16:16	6.7	4315	1.002635
E	14	9:04	5.2	1546	1.000953
		10:30	6.1	1751	1.001058
		11:56	6.7	1615	1.000950
		13:31	5.9	1925	1.001172
		14:57	5.3	3065	1.001899
		16:16	5.3	3929	1.002438
		17:04	4.9	3948	1.002457

Table 1 Continued.

Sampling Point	Day	Time	Water Temp. (°C)	Sediment Conc. (mg/l)	Density (g/cm³)
E	15	8:56	5.0	2938	1.001825
		10:56	6.7	2980	1.001803
		12:01	7.2	3745	1.002257
		14:56	5.0	9280	1.005783
		16:20	3.3	10670	1.006652
E	16	7:54	2.8	11900	1.007415
		8:51	2.7	11100	1.006914
		9:50	2.9	10610	1.006611
C	17	11:26	4.0	2769	1.001728
D		11:38	4.0	1690	1.001054
E		11:51	5.6	3746	1.002317
F		13:58	7.7	3669	1.002183
F		15:01	6.5	3277	1.001996
F	19	8:53	4.4	2245	1.001399
		10:32	4.7	1959	1.001218
		11:57	5.0	1893	1.001173
		14:07	4.9	1640	1.001017
F	21	8:31	2.9	293.5	1.000174
		10:24	3.8	309.0	1.000193
		12:25	5.1	286.5	1.000169
		14:00	5.8	246.5	1.000128
F	22	14:30	8.0	113.0	0.999947
	25	14:50	8.0	65.0	0.999917
	26	14:50	6.0	127.0	1.000047
	28	13:00	4.5	290.0	1.000179
	29	11:02	6.7	226.5	1.000084

outflow of reservoir water recorded every hour by the Control Office of the reservoir. Temperature of river water was recorded continuously by the bimetal recording thermometer at the F point (solid thick line), and furthermore measured by the rod thermometer at every time of sampling (dashed line). Density in Table 1 is bulk density and was obtained by eq. (1).

$$\rho_{\theta c} = (1 - C \times 10^{-6}/\rho_s)\,\rho_\theta + C \times 10^{-6} \qquad (1)$$

$\rho_{\theta c}$: bulk density, C: sediment concentration, ρ_s: density of particles (=2.6616 g/cm³ for reservoir sediments), ρ_θ: density of pure water at θ°C

Sediment concentration and river discharge increased gradually from April 13 and reached the maximums on April 16, followed by gradual decrease to April 20. And thereafter up to April 29 no sediment discharge occurred

conspicuously. The maximums of sediment concentration and discharge were 11,900 mg/l and 45.11 m^3/s respectively, and sediment concentration more than 10,000 mg/l lasted about 18 hours from April 15 to 16, which can be caused by warmer weather on April 15 that represented air temperature higher than 0°C even on the night, and rainfall on April 16.

The maximums of sediment concentration happened prior to that of discharge by about an hour. The shift in time of the two peaks is already pointed out by Hjulström[17] and will be explained as the result that the peak velocity of flood flow preceded its peak discharge in time[18].

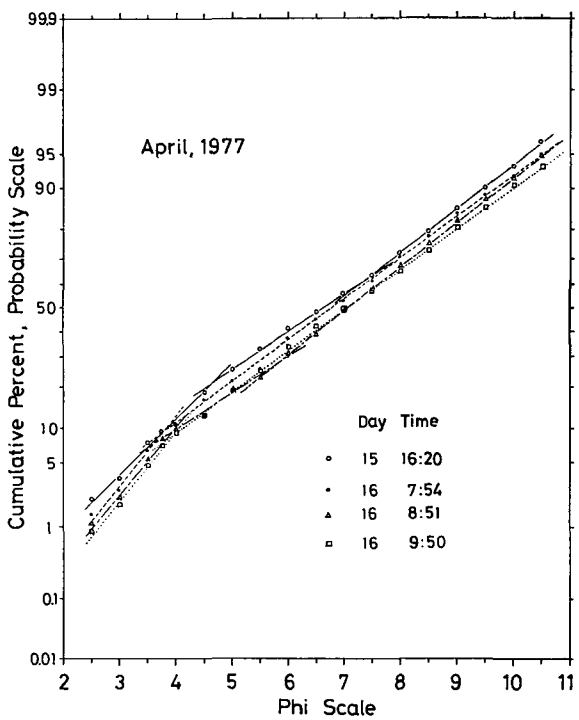

Fig. 3 Grain-size distributions of suspended sediments in river water at about the time of the peak concentration.

Fig. 3 indicates grain-size distributions of suspended sediments in river water at about the time of the peak concentration. These were analyzed by the photo-extinction method with a centrifuge ($\phi > 3.75$) and the sieving method ($\phi < 3.75$).

The distributions show that the suspended sediments consist of more or less 90 per cent of silt and clay ($\phi>4$) in weight, and a break point is located at about $\phi=4$ on log-probability paper, which distinguishes the sediments into the two subpopulations correspondent to each of the limits of "suspended load" ($\phi<4$) and "wash load" ($\phi>4$).

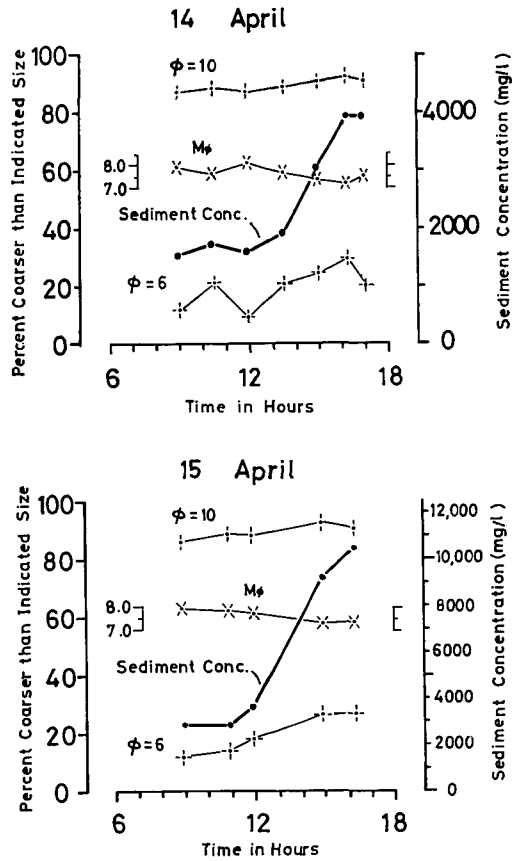

Fig. 4 Changes with time of sediment concentration, the percentage in weight of suspended sediments correspondent to $\phi<6$ and $\phi<10$, and mean phi (M_ϕ) on April 15 and 16.

Fig. 4 indicates changes with time of sediment concentration, the percentage in weight of suspended sediments corresponding to $\phi<6$ and $\phi<10$ and mean phi ($M_\phi=(\phi_{84}+\phi_{16})/2$) on April 15 and 16. Good correlations between sediment concentration and the percentage of $\phi<6$ show distinctly that the

higher sediment concentration, the more the number of coarser sediments, and however, little change of the percentage of $\phi<10$ resulted in only a little change of M_ϕ with sediment concentration.

Fig. 5 indicates hydrological records of the reservoir during the period January 1 to June 30, 1977. As a result, the peak discharge observed on April 16 was the maximum inflow of Katsurazawa Reservoir during the period of snow melting of the year 1977.

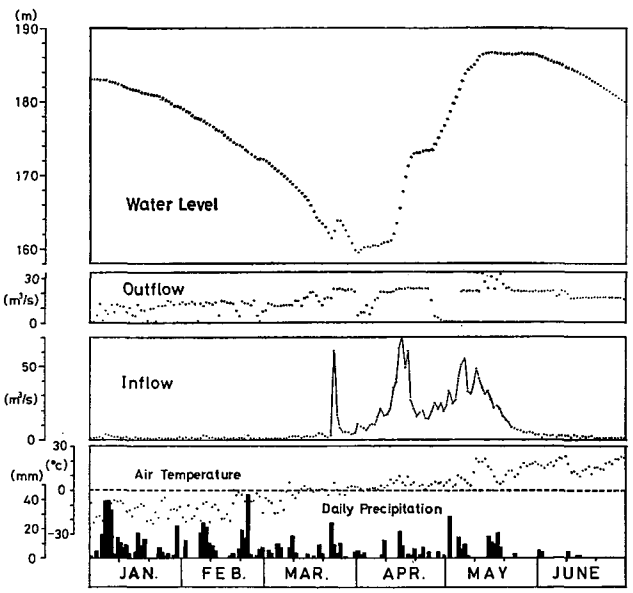

Fig. 5 Hydrological records during the period January 1 to June 30, 1977.

2.2 *Intrusion pattern of melting water flowing into the reservoir*

How the reservoir will respond to sediment discharge of influent river during the period of spring thaw was examined by sampling reservoir water from or at near the dam shown by the point of A in Fig. 1. Sampling was performed on April 29, 1977 and on March 29, 1978 falling on the latter-half day and the early day respectively during the snow-melting period. The observation of reservoir water on March 29, 1978 was made at three points on the ice about 120 m upstream from the dam.

Table 2 indicates the results of sampling. The data under date of March 29, 1978 are those obtained at the deepest point.

Table 2 Observational results of reservoir water under date of April 29, 1977 and March 29, 1978.

April 29, 1977

Inflow Water				
Point	Time	Water Temp. (°C)	Concentration (mg/l)	Density (g/cm³)
F	11:02	6.7	226.5	1.000084
Reservoir (w.l.=175.62 m)				
Water Depth (m)		Water Temp. (°C)	Concentration (mg/l)	Density (g/cm³)
0		4.3	116.5	1.000072
2		5.0	125.0	1.000070
4		4.0	45.0	1.000028
6		3.8	116.0	1.000072
8		3.8	114.0	1.000071
10		3.8	206.5	1.000129
12		3.0	321.0	1.000193
14		3.0	410.0	1.000248
18		3.3	707.5	1.000438
22		3.2	846.5	1.000523
26		3.3	—	—
30		3.2	1520	1.000943
32		3.3	—	—
33		3.2	1705	1.001059
33.72 (bottom)		3.2	1795	1.001115

The surface layer of the depth 0 to 8 m remained rather dilute with turbidity of 45.0 to about 120 mg/l during the period of snow melting. However, on account of the difference in water level, the depth 8 m on March 29 corresponds to that of 19.69 m on April 29 as to height above the sea-level, and as a result the whole reservoir water observed on March 29, especially the bottom layer, turned so turbid as snow melting progressed. This may be explained by deposition of almost all suspended sediments in reservoir water during the period of low water of river from November of the preceding year to March of the year which is followed by occurrence of such turbidity currents as underflows with considerable sediment discharge during the snow-melting period.

The river water on April 29 was sampled at the F point and that on March 29, at the E point. The results of inflow water are also shown in Table 2.

It is seen that since pure water has the maximum density at 4°C, the difference of temperature between river and reservoir waters shown in Table 2

Table 2 Continued.

March 29, 1978

Inflow Water				
Point	Time	Water Temp. (°C)	Concentration (mg/l)	Density (g/cm³)
E	16: 00	0.51	1633	1.000919
Reservoir (w.l. = 163.93 m)				
Water Depth (m)		Water Temp. (°C)	Concentration (mg/l)	Density (g/cm³)
0		0.15	—	—
0.5		0.11	—	—
1		0.12	—	—
2		0.20	85.0	0.999934
3		0.23	—	—
4		0.28	—	—
5		0.33	96.0	0.999949
6		1.99	—	—
7		1.98	56.0	1.000002
8		2.14	—	—
9		1.23	—	—
10		1.51	153.5	1.000046
12		2.91	141.0	1.000079
13		3.23	182.5	1.000109
14		5.06	—	—
15		—	303.0	—
16		5.36	311.5	1.000179
17		5.37	—	—
18		5.37	311.5	1.000179
20		5.37	348.5	1.000203
22		5.37	—	—
24		5.38	362.0	1.000210
25		5.39	350.5	1.000203
26		5.40	—	—
26.85 (bottom)		5.40	—	—

will have no great influence on the density difference between the two waters. As the result, a difference of sediment concentration will almost control a difference of bulk density between the two waters.

The river water on April 29 had lower concentration than that of the bottom layer of the reservoir, and however higher than that of the surface layer, so that the water would have flown down as underflows to the depth about 8 m and then have intruded into the reservoir as interflows.

The inflow water on March 29 had concentration by far higher than that of the whole reservoir water. The river water would have resulted in such turbidity currents as underflows flowing down to the dam, even if taking

sedimentation in course of flowing into account.

As the above result, it was seen that sediment concentration of river water would almost control intrusion pattern of flow into the reservoir during the period of spring thaw.

Table 3 indicates flow pattern of melting water in the reservoir separated by sediment concentration observed. The patterns were determined in consideration of a difference of bulk density between river water and surface-layer water of the reservoir, and the changes of water level and concentration of the lower layer of the reservoir. Bulk density (ρ_θ) of surface-layer water of the reservoir was calculated as C=100 mg/l and temperature equal to that of inflow water by eq. (1).

Table 3 Flow pattern in the reservoir separated by sediment concentration observed.

C (mg/l)	θ (°C)	$\rho_{\theta c}$ (g/cm³)	Q (m³/s)	w.l. (m)	ρ_θ (g/cm³)	Flow Pattern
65.0	8.0	0.999917	9.50	173.30	0.999938	overflow
109.0	1.7	1.000025	5.47	160.82	1.000020	
226.5	6.7	1.000084	7.16	175.58	1.000005	underflow→interflow
309.0	3.8	1.000193	5.84	173.04	1.000062	
412.0	5.9	1.000228	6.72	160.87	1.000034	
524.5	5.6	1 000307	5.04	160.93	1.000042	
606.0	5.9	1.000349	6.70	160.93	1.000034	
684.0	7.3	1.000342	6.82	160.88	0.999977	underflow
830.0	4.6	1.000515	8.39	161.29	1.000059	
920.5	6.0	1.000543	7.25	160.43	1.000030	
1389	8.0	1.000743	14.94	161.45	0.999939	
1633	0.5	1.000919	5.27	163.93	0.999962	
1959	4.7	1.001218	9.67	172.19	1.000058	underflow→interflow
3065	5.3	1.001899	14.87	163.00	1.000049	
9280	5.0	1.005783	21.36	164.67	1.000054	underflow to the dam
11900	2.8	1.007415	45.11	166.48	1.000051	

At $C<100$ mg/l, river water will always flow into the reservoir as overflows during the snow-melting period (Table 2).

At $100<C<400$ mg/l, inflow water will behave as underflows in the upstream reach of the reservoir, and however on account of sedimentation by the flows and/or the appearence of the lower layer with higher concentration in the reservoir as snow melting progressed, the flows will turn into interflows at a comparatively small depth.

At $400<C<3{,}000$ mg/l, inflow water will flow down on most of the reservoir beds as underflows. However, inflow water of 1959 mg/l, which was observed on April 19 after the peak sediment discharge, will turn into interflows in the mid-stream reach of the reservoir, because considerable sedimentation in course of flowing results from the increase of a flowing distance with water level, and the lower layer with much higher concentration increases in thickness.

At $C>3{,}000$ mg/l, regardless of the increase of sediment concentration of reservoir water with the progress of snow melting, inflow water will result in turbidity currents reaching the dam as underflows.

2.3 Comparison with the period of rainfall runoff

How the reservoir will be influenced by rainfall runoff is shown in Fig. 8 in the previous paper.[7)]

During the period of rainfall runoff, the reservoir have the bottom-layer water much denser than river water in low stage, which results from suspension of a number of fine-textured sediments, attributed to intrusion of turbid water into the reservoir during the period of spring thaw.

During the surveying period August 20–22, 1975, water temperature of the Ikushunbetsu River (see Fig 1) was 20.02°C on the average, and on the other hand, turbidity and water temperature of the bottom layer near the dam were about 1,200 mg/l and 7.5°C respectively. As a result, since waters of the bottom layer have bulk density of 1.000654 g/cm^3, river water with 20.2°C must have turbidity of 3950 mg/l in order to become equal to its bulk density. In consideration of sedimentation while flowing in the reservoir, some lowering of inflow-water temperature in torrential runoffs and the finer texture of suspended sediments in river water, inflow water with turbidity of about 6,000 mg/l will first turn into turbidity currents flowing down to the front of the dam as underflows. Actually, inflow water in torrential runoffs except for such an example as that on August 23, 1975 will almost result in interflows in the reservoir (see Fig. 2 in the previous paper[7)]).

In case of the snow-melting period, turbidity currents reaching the dam as underflows could occur through inflow of river water with turbidity or concentration of more than about 3,000 mg/l. The period of spring thaw, compared with that of torrential runoffs, can offer the circumstances of reservoir and river fully suitable for remarkable occurrence of turbidity currents.

3. Experimental study

Laboratory experiment is subsequently attempted to elaborately investigate the sedimentary mechanism of turbidity currents.

3.1 Apparatus and procedure

Apparatus – The experiments are performed in a recirculating flume, 500 cm long, 40 cm deep and 30 cm wide with plane bed (Fig. 6). The flume is constituted by a steel floor and both sides of hard glass, 10 mm thick and can be tilted by a jack. A headbox and a tailbox are in the upstream and the downstream respectively, and a stirrer is set up in each box to keep suspended sediments in water from deposition.

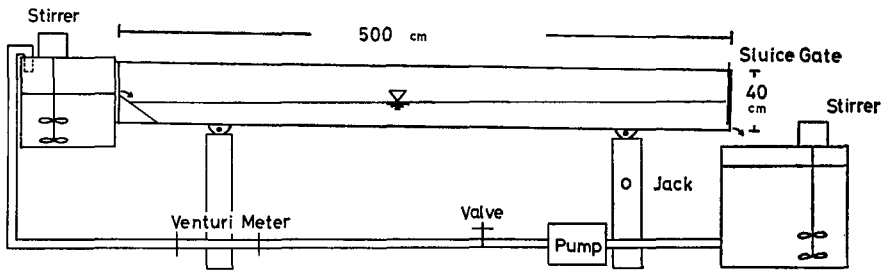

Fig. 6 Experimental flume, 500 cm long, 40 cm deep, and 30 cm wide constituted by a steel floor and both sides of hard glass, 10 mm thick.

Discharge is controlled by a valve and flow rate is measured by a venturi meter. A venturi meter is connected by two tubes with a manometer, and has a "shell" of aluminum inside a pipe by which a difference of pressure can be generated (Fig. 7). A systematic correlation between flow rate and the reading of manometer was previously obtained by a preliminary experiment in open channel.

Sampling of turbid water flowing in mixing zone or as turbidity currents is performed by an unique water sampler of plastics (Fig. 8), designed by the writer and consisted of double pipes. The inner pipe is partitioned by plastic walls into some rooms, and both pipes have rectangular holes penetrated in same size. In sampling water, the outer pipe is fixed in a flume, and then the closing of the holes is made by the revolution of 90° of the inner pipe by a "finger-knob", at a given time when turbid water is passing around and through the sampler. Thus turbid water of each layer in mixing zone or

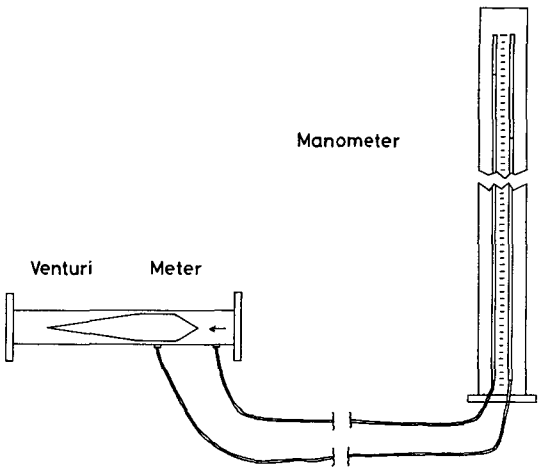

Fig. 7 Venturi meter connected with a manometer by two tubes.

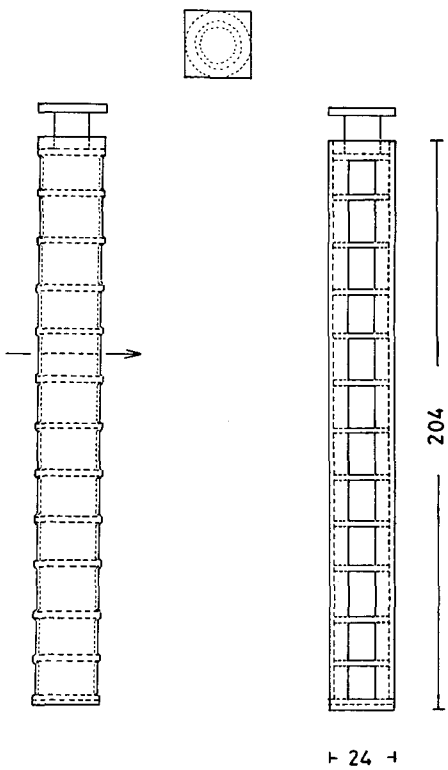

Fig. 8 Water sampler of plastics. Length is shown in millimeters.

turbidity currents, where suspended sediments are actively depositing, could be sampled instantaneously at a given point in flume.

Vertical distributions of flow velocity in mixing zone and turbidity currents, are obtained by a flowmeter made by the writer.

Fig. 9 indicates a sensor of the flowmeter. The measurement was made moving up and down the sensor fixed to a point-gauge. The flowmeter is used by Ashida and Egashira[12] and based on the recording of a difference of electric resistence between tap water and salt water. Salt water flows out in the upstream direction from a pipe, 15.5 mm distant from the upper electrodes. The time which salt water spent in crossing a pair of electrodes upstream and then another downstream is recorded on a chart as the distance between two pulses corresponding to the two pairs.

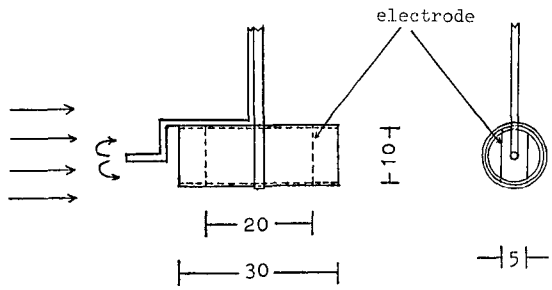

Fig. 9 Sensor of a flowmeter. Length is shown in millimeters.

On the other hand, a water-soluble pigment of Nigrosine was dropped at the upstream end of flume, and the maximum velocity of turbidity currents was measured.

Comparison of the results with that by the flowmeter showed the average deviation of 2.0%.

Procedure – Tap water is poured into a flume up to such a water level as plunging point, during the experiments, will be located at a point approximately 100 cm downstream from the end of flume. And then under a previous fixation of flow rate, turbid water with a given concentration is flown into a tilted flume from a headbox with two stirrers operated.

The turbid water is mixed with tap water in the upstream of flume, followed by its plunging at a point and then occurrence of turbidity currents. The head of formed turbidity currents flows down on the floor of flume and immediately on its reaching the downstream end, the sluice gate is opened.

Turbid water is thus returned to the tailbox and then pumps again to the headbox. Since on account of sedimentation in flume the turbid water restored was diluted, original materials were added at constant rate to the water in the tailbox.

In course of the circulation of turbid water, measurements of flow velocity and water sampling were performed. Water sampled was later analyzed for concentration and grain size of suspended sediments in its water.

Immediately after the stop of discharge into the flume, waters in flume are drained by the opening of sluice gate.

The sediments deposited in flume were sampled and analyzed for grain size.

3.2 Results

Table 4 indicates the conditions of the experiments shown as examples and the main parameters on grain size of original materials used for them. As the materials used was artificial powder of silica which consists of lots of silt and clay and has a wide distribution of grain size, with density of 2.656 g/cm^3 which is almost equal to that of the bottom sediments of Katsurazawa Reservoir. The percentage in weight of $d>74\ \mu$ ($\phi<3.75$) in Table 4 is, as mentioned below, an important parameter related to a different mode of sediment transport and deposition in mixing zone and turbidity currents. The concentration in Run 18 was the highest of all the experiments.

Table 4 Conditions of the experiments shown as examples and the main parameters on grain size of original materials used for them. (I: bottom slope, Q: flow rate, C: concentration of inflow water, T: water temperature; d_m: median diameter of original materials, σ_ϕ: standard deviation $(=1/2\cdot(\phi_{84}-\phi_{16}))$)

Run	I	Q (cm^3/s)	C (mg/l)	T (°C)	d_m (μ)	σ_ϕ	$d>74\ \mu$ (%)
10	0.010	1610	9870	15.2	2.30	1.58	14.10
18	0.020	1200	24600	15.6	2.94	1.12	8.71

Fig. 10 indicates grain-size distributions of original materials used in Run 10 and Run 18. Characteristically, the distributions for Runs 10 and 18 have two and three break points respectively on log-probability paper.

Fig. 11 indicates vertical distributions of velocity and concentration in Run 10. Sampling of turbid water is made at Points 2, 3 and 5, and measurements of velocity, at Points 3 and 5. Points 2, 3 and 5 are 180, 230 and

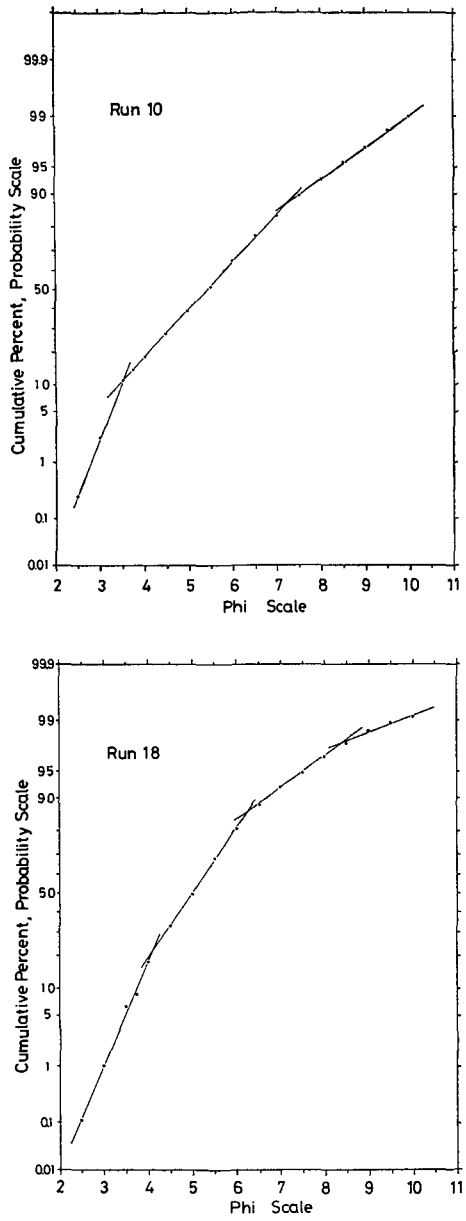

Fig. 10 Grain-size distributions of original materials used in Run 10 and Run 18.

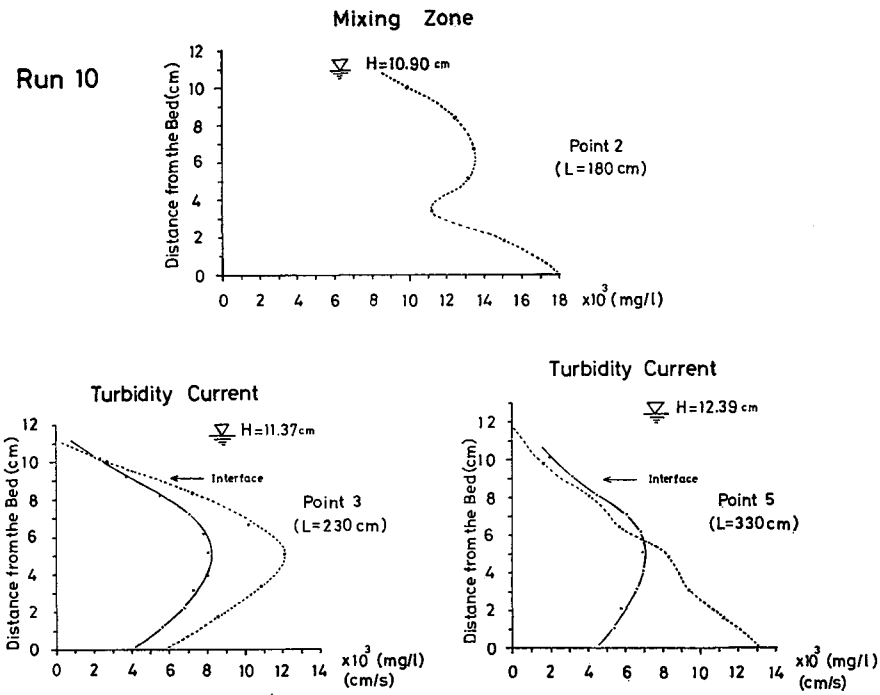

Fig. 11 Vertical distributions of velocity (solid line) and concentration (dashed line) in Run 10.

330 cm respectively distant from the upstream end of flume.

In the experiments, plunging point was located at the distance of 203 cm, and as a result Point 2 was positioned in mixing zone, and Points 3 and 5, in a zone of turbidity currents.

Generally, vertical profile of concentration in mixing zone is in shape irregular but similar to that of velocity. The example in Fig. 11 has two maximums of concentration at Point 2. The turbidity current at No. 3 has the maximums of concentration and velocity at almost the same depth, and an inflection point of the velocity profile near the boundary between fresh and turbid waters. As well as the experimental results by Lofquist[19] and Ashida and Egashira[12], the inflection point is defined as the interface of turbidity currents. At Point 5, the concentration and velocity distributions approach to those of turbidity currents of uniform flow, and the inflection point of velocity profile comes to appear more clearly.

Fig. 12 indicates vertical distributions on grain size of the suspended sediments in mixing zone and turbidity currents in Run 10. In mixing zone, the nearly uniform distribution, on the whole, is seen but the two points in depth with the maximum concentration, shown in Fig. 11, conform to those with the coarser maximum of size frequency for silt ($8.0>\phi>4.0$).

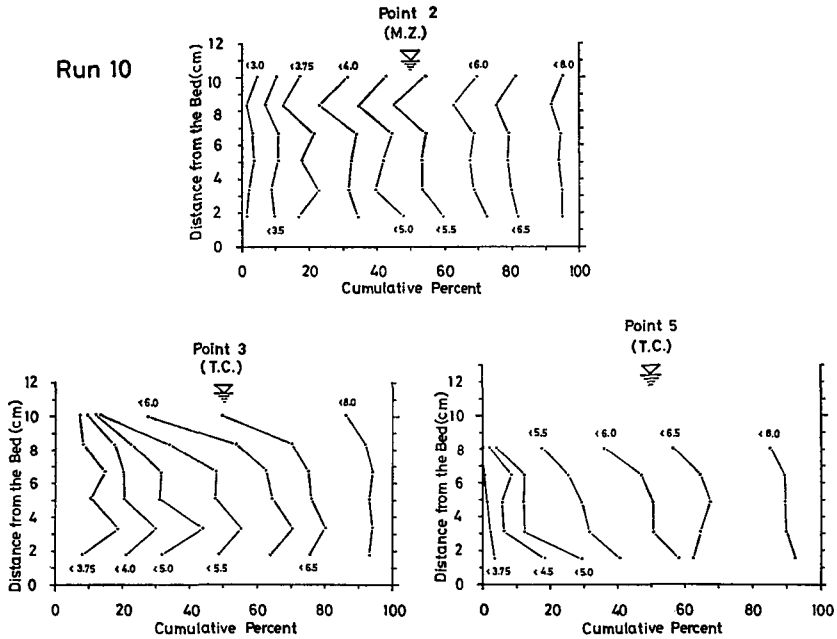

Fig. 12 Vertical distribution on grain size of the sediments suspended in mixing zone and turbidity currents in Run 10.

In turbidity currents, as flowing to the downstream, the suspended sediments of sand size decrease abruptly in amount, especially at near the interface and those of silt size come to constitute the large percentage, and on the other hand coarser sediments of $\phi<5.0$ become concentrated towards the bottom.

Fig. 13 indicates vertical distributions of velocity and concentration for Run 18. In this experiment, plunging point was positioned at the distance of 100 cm, and as a result all the measuring points were existed in turbidity currents. On account of the so high concentration of inflow water, the change of vertical profiles of concentration with time is comparatively great at each point, especially at Point 2. The change at Point 6 resulted from the

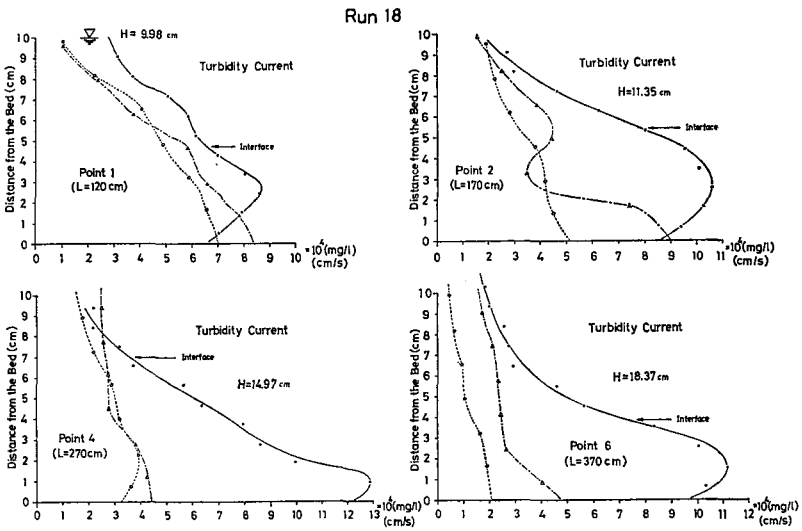

Fig. 13 Vertical distributions of velocity (solid line) and concentration (dashed line) in Run18. ○ and △ are the results before and after the measurement of velocity respectively.

impact between the upper boundary of turbidity currents and the lower end of sluice gate. Nevertheless, the interface at Points 2 and 6 could be confirmed clearly due to the fine velocity profiles. On the other hand, since the shapes of the velocity profiles at Points 1 and 4 are anomalous, as the interface is determined the point at which inflection of velocity and/or concentration profiles are located and the shapes of grain-size-distribution curves of suspended sediments change abruptly on log-probability paper.

Fig. 14 indicates grain-size distribution of the bottom sediments in mixing zone of Run 10. The distribution pattern is similar to that on original materials, and however the values of median diameter, standard deviation and grain size corresponding to two break points, and the percentage in weight of $d>74$ μ are different from those for the original materials (Fig. 10 and Table 5). The break points for the bottom sediments always appeared on log-probability paper, regardless of the existence of those for the original materials, and therefore can be considered to result from truncation of log-normal distributions corresponding to three subpopulations, which are each related to different modes of sediment transport and deposition[20),21)] The three modes are also shown in Fig. 14.

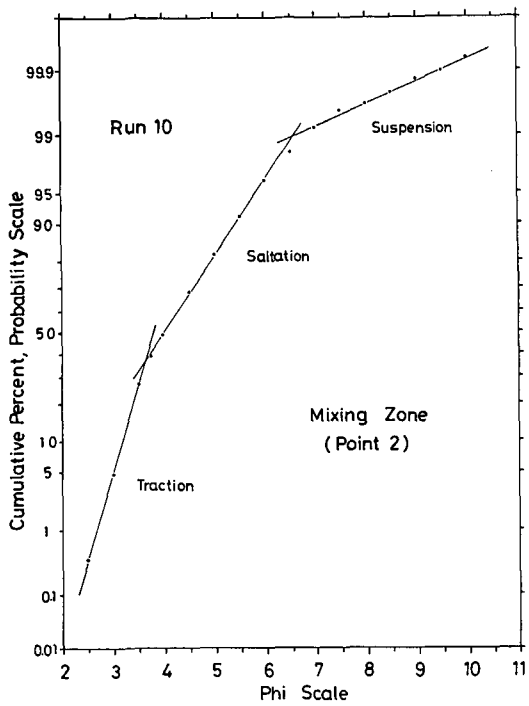

Fig. 14 Grain-size distribution of the bottom sediments in mixing zone of Run 10.

Table 5 Important parameters on grain size of the bottom sediments shown in Figs. 14 to 17.

Run 10					
Point	Md_ϕ	σ_ϕ	Coarser Break (ϕ)	Middle Break (ϕ)	Finer Break (ϕ)
2	4.03	0.885	3.65	6.69	—
3	4.42	0.750	3.00	4.71	6.76
5	4.69	0.735	3.47	4.92	6.81
6	4.80	0.665	3.74	4.89	6.95
Run 18					
Point	Md_ϕ	σ_ϕ	Coarser Break (ϕ)	Middle Break (ϕ)	Finer Break (ϕ)
1	4.47	0.860	3.60	6.83	—
2	4.64	0.860	3.88	6.86	—
3	4.70	0.790	3.00	4.13	6.75
4	4.83	0.770	3.12	4.52	6.93
5	4.97	0.755	3.60	4.53	6.75
6	5.05	0.725	3.64	4.71	6.51

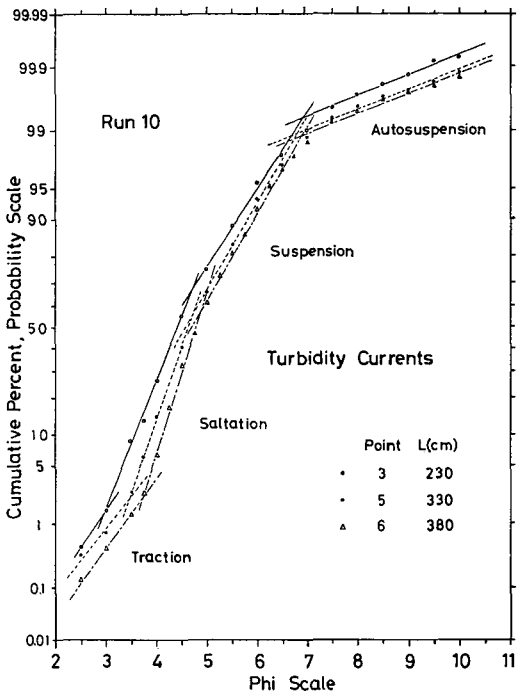

Fig. 15 Grain-size distributions of the bottom sediments in turbidity currents of Run 10.

With reference to the study by Sagoe and Visher[22], the break between traction and saltation populations is named "coarser break" and that between saltation and suspension populations, "middle break".

Fig. 15 indicates grain-size distributions of the bottom sediments in turbidity currents of Run 10. All the log-probability plots have three break points, dividing the sediments into four subpopulations. Coarser and middle breaks show the gradual increase in phi scale towards downstream and however, "finer break" between suspension and "autosuspension" populations hardly shifts on grain size.

The conception of "autosuspension" was suggested by Bagnold[23], who proved theoretically that no suspended sediments in turbulent water settled on the bottom on account of upward turbulence produced by the particles themselves. Further details will be furnished in the following section.

Fig. 16 indicates grain-size distributions of the bottom sediments sampled

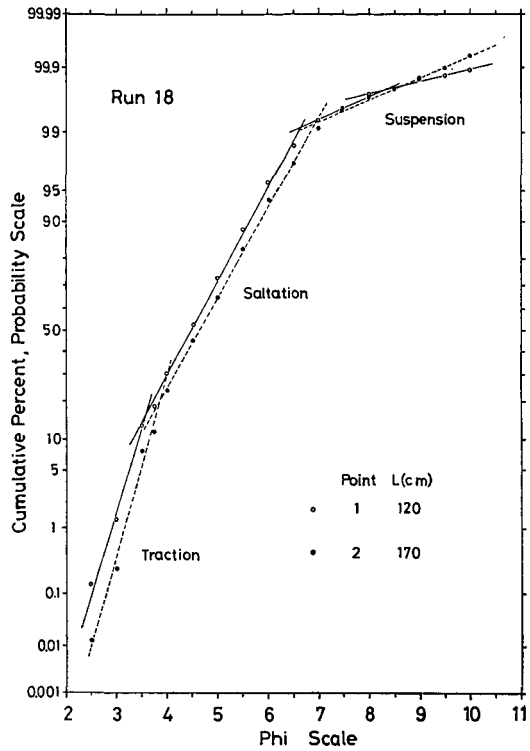

Fig. 16 Grain-size distributions of the bottom sediments sampled at Points 1 and 2 in Run 18.

at Points 1 and 2 in Run 18. Despite location of the two sampling points in turbidity currents, the log-probability plots of the sediments show the three subpopulations characteristic of those in mixing zone. This can be caused by the so high concentration of flowing water and the greater height from bottom to maximum-velocity point at Points 1 and 2, resulting in the greater shear stress at the bottom (Fig. 13). Only one break in the log-probability plots of suspension population occurred at Point 1, which is due to the characteristic of grain-size distribution of the used original materials (Fig. 10).

Fig. 17 indicates grain-size distributions of the sediments in the downstream from Point 3. The bottom sediments consist of four subpopulations peculiar to those in turbidity currents, and save those at Point 3 have likewise one or two break points in the log-probability plots of suspension population.

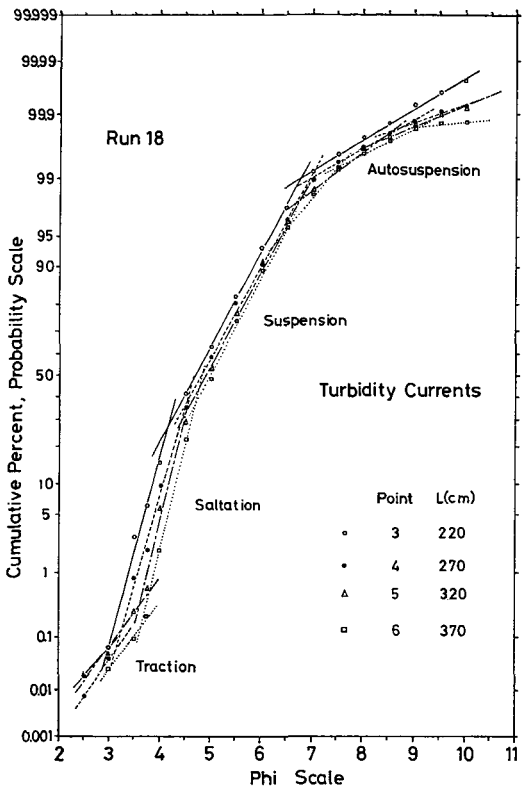

Fig. 17 Grain-size distributions of the sediments in the downstream from Point 3 in Run 18.

The values of median phi and in phi scale of coarser and middle breaks increase gradually towards downstream, and however the finer breaks show a fluctuation on grain size.

Table 5 indicates the important parameters on grain size of the bottom sediments. All the parameters change abruptly at or near plunging point. This can be attributed to the difference in flowing and sedimentary mechanisms between mixing zone and turbidity currents. Flow in mixing zone should be treated as suspension flow in open channel[11].

3.3 Discussion

Fig. 18 indicates grain-size distributions of all the suspended sediments at each of the gauging points in Run 10. Each of the two or three break

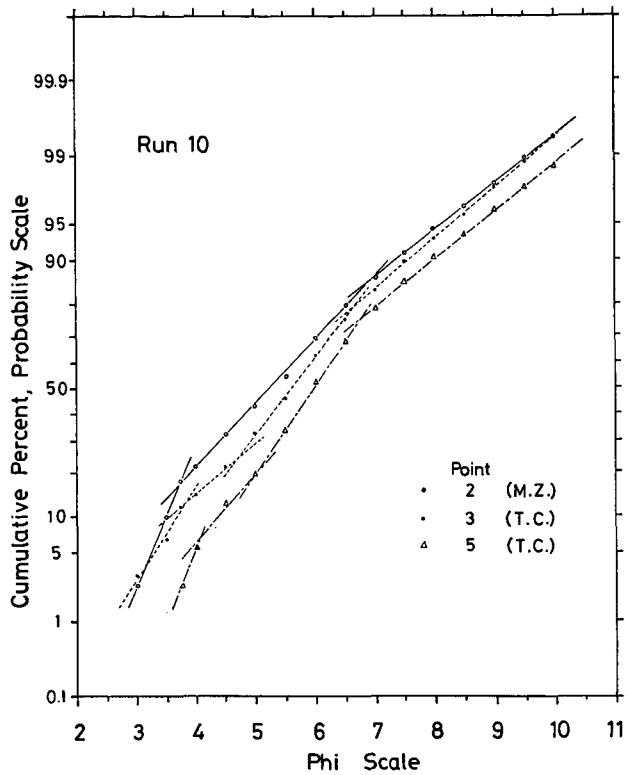

Fig. 18 Grain-size distribution of all the suspended sediments at each gauging point of Run 10.

points in log-probability plots can correspond to each of those for the bottom sediments at the same points. And furthermore the tendency to downstream increase or decrease in value of the parameters shown in Table 5 is equivalent to that for the bottom sediments.

Fig. 19 indicates vertical distributions of the parameters on grain size of the suspended sediments in relation to the result shown in Fig. 12. The parameters were calculated by eqs. (2), (3) and (4)[24].

$$\text{Mean Phi:} \quad M_\phi = (\phi_{84}+\phi_{16})/2 \tag{2}$$

$$\text{Skewness :} \quad \alpha_\phi = (M_\phi - Md_\phi)/\sigma_\phi \tag{3}$$

$$\text{Kurtosis :} \quad \beta_\phi = \{(\phi_{95}-\phi_5)/\sigma_\phi - 1\}/2 \tag{4}$$

As the result, the suspended sediments sampled near the bottom has

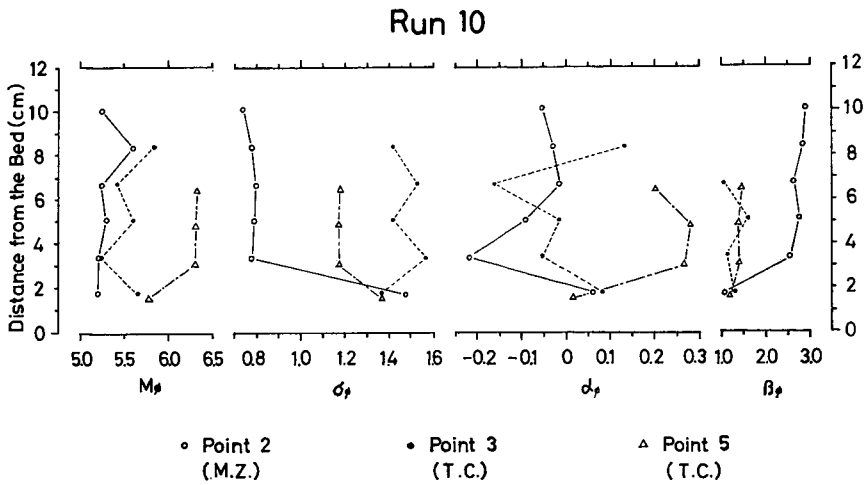

Fig. 19 Vertical distributions of the parameters on grain size of the suspended sediments in relation to the result shown in Fig. 12.

the same tendency as the bottom sediments as to the shifts of the parameters towards downstream. The above results can lead to the conclusion that at a given point in mixing zone and turbidity currents, the fluid properties of flow, the vertical distribution of flow velocity and the bottom shear stress will control the proportion of mixture among the three or four subpopulations of suspended sediments near the bottom and as the result the shape of grain-size-distribution curves on log-probability paper for the sediments.

It was thus attempted to grasp the sedimentological significance of each break in log-probability plots by introduction of eqs. (5), (6) and (7).

$$F_r = u/\{(\rho_{\theta c}-\rho_\theta)\, gh/\rho_{\theta c}\}^{1/2} \tag{5}$$

$$Re = u_{*b}\cdot d/\nu \tag{6}$$

$$u_{*b} = \{(\rho_1-\rho_\theta)\, gh_1 I/\rho_1\}^{1/2} \tag{7}$$

u: a mean velocity of flow in mixing zone and turbidity currents (cm/s), $\rho_{\theta c}$, ρ_θ: bulk density of flowing water and clear water respectively (g/cm^3), h: height of flow from bottom to water surface in mixing zone and to interface in turbidity currents (cm), g: acceleration due to gravity (cm/s^2), u_{*b}: friction velocity at the bottom (cm/s), d: a grain diameter of the bottom sediment correspondent to a break point (cm), ν: kinematic viscosity (cm^2/s), ρ_1: bulk density of flowing water from bottom to

maximum-velocity point (g/cm^3), I: bottom slope, h_1: height from bottom to maximum-velocity point (cm)

Re is the Reynolds number on particle.

Fig. 20 indicates the relation between Fr and Re for coarser break, obtained from the present experiments. The negative correlation between the two is evident. On the other hand, the positive correlation of u with u_{*b} is ascertained through all the experimental results. Therefore it is seen that even the more fine-grained sediments come to be transported by the means of traction with the increase of flow velocity, namely a power of sediment transport.

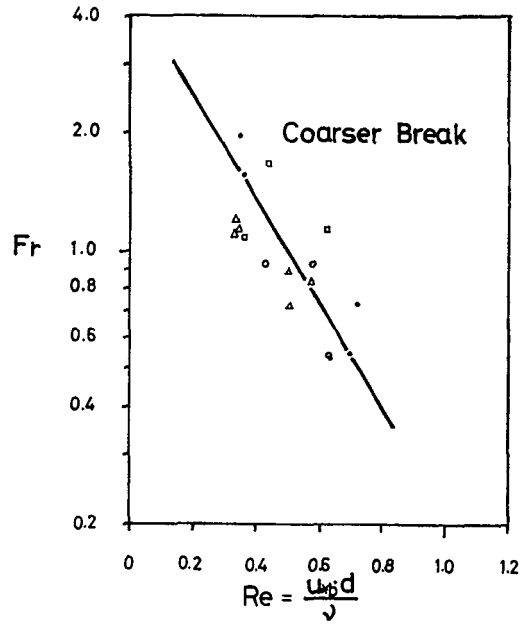

Fig. 20 Relation between Fr and Re for coaser break.

Fig. 21 indicates the "Shields curve" (thick line) showing the relation between the two dimensionless parameters of critical tractive force. Shields curve has been obtained empirically by the laboratory experiments with open channel, and the curves C and C′ can be used separately according to the experimental results. The relation is called "Shields relation" and represented by eq. (8) (see p. 79–86 in the Yalin's paper[25]).

$$Y_c = \frac{\rho_\theta u_{*c}^2}{(\rho_s - \rho_\theta) gd} = f(X_c) = f\left(\frac{u_{*c} d}{\nu}\right) \tag{8}$$

ρ_s, ρ_θ: density of particle and flowing water at θ°C respectively (g/cm^3),
u_{*c}: critical friction velocity (cm/s)

According to the result in Fig. 20, a grain size (d) correspondent to coarser break is considered to be equivalent to a critical grain size of the sediments transported by the means of traction. Therefore all the plots in Fig. 21 were obtained as $u_{*c}=u_{*b}$ for mixing zone (black) and turbidity currents (white).

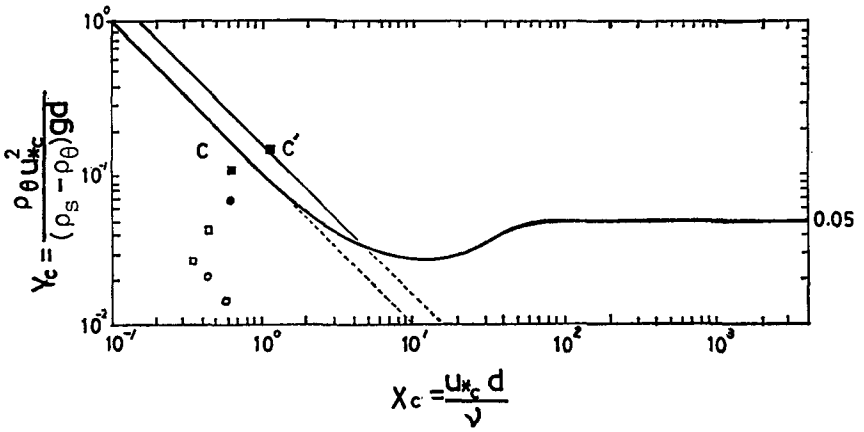

Fig. 21 Shields curve showing the relation between the two dimensionless parameters of critical tractive force after Yalin[25]. The black and white plots are those for mixing zone and turbidity currents respectively.

As the result, the plots for mixing zone are positioned on or near Shields curve, showing the characteristic of flow in open channel, and those for turbidity currents go away from the curve, indicative of its relation peculiar to turbidity currents. This, as well as the result seen in Table 5, implies the difference in flowing mechanism and sedimentation between mixing zone and turbidity currents. However, in general the obtained tractive force will be underestimated because u_{*b} at cessation of sediment transport is smaller than u_{*c} at its initiation (Sundborg[26], p. 181; Francis[27], p. 457). All the plots are within the limits showing the negative correlation between the two dimensionless parameters on Shields curve, which shows the validity of the result seen in Fig. 20.

Fig. 22 indicates the relation of Fr with the Reynolds number on particle correspondent to middle break. The correlation between the two parameters is positive and higher than that in case of coarser break. This shows that the more coarse-grained sediments can be transproted and deposited by the means of suspension with the increase of flow velocity or tractive force, because suspension rather than saltation can be directly controlled in motion by the turbulence[27),28)].

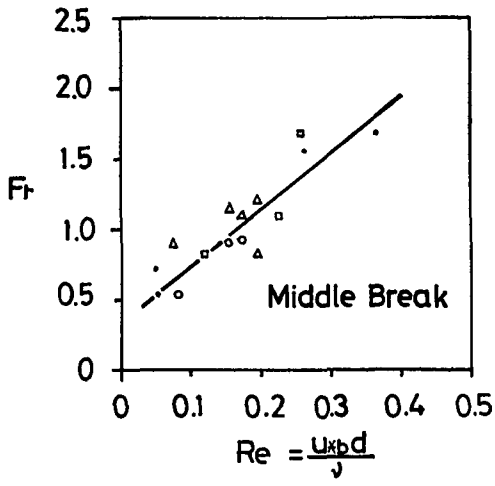

Fig. 22 Relation of Fr with Re for middle break.

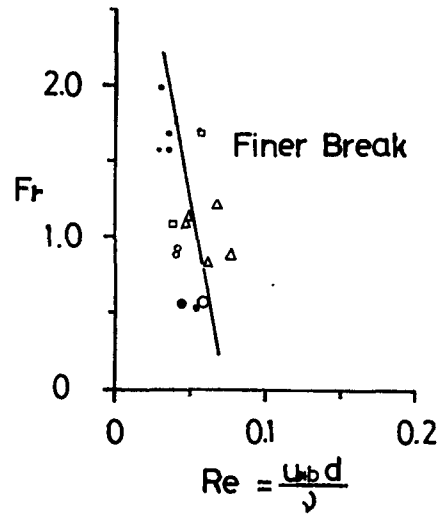

Fig. 23 Relation of Fr with Re for finer break.

Fig. 23 indicates the relation of Fr with Re correspondent to finer break which can appear only in turbidity currents. The correlation between the two parameters is barely or ambiguous. This may be caused by the collective influence of not only the two parameters but all the others characteristic of flow in turbidity currents on the suspended sediments finer than those of a grain size corresponding to finer break. The occurrence of finer break will be explained, in the following, by the application of "autosuspension model" to the suspended sediments in turbidity currents.

Fig. 24 indicates transport rate for each grain-size fraction of all the suspended sediments at each gauging point in Run 10.

The overlapping of curves corresponding to greater than about 6.5ϕ shows that no suspended sediments finer than those of some 6.5ϕ are almost deposited

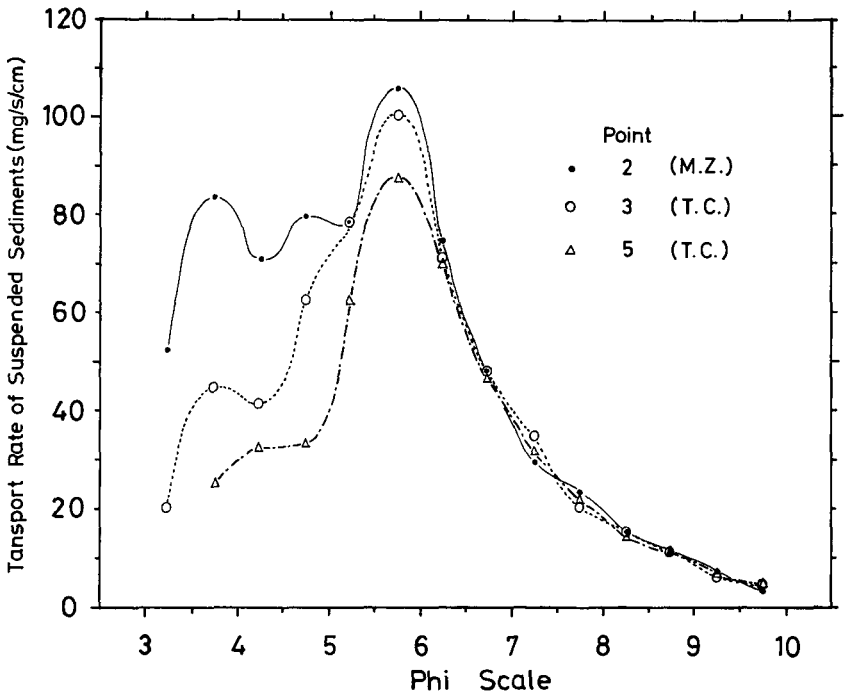

Fig. 24 Transport rate for each grain-size fraction of all the suspended sediments at each gauging point in Run 10.

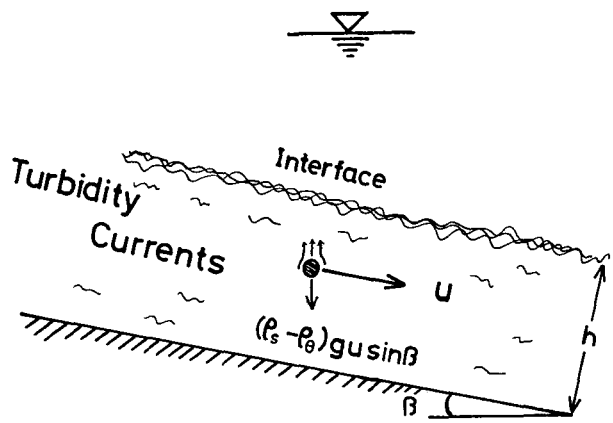

Fig. 25 Autosuspension model after Bagnold[23], applied to turbidity currents.

towards downstream. The value of 6.5ϕ is nearly equal to the grain size of finer break. Therefore the explanation of no deposition of such suspended sediments will lead to clarify the sedimentological significance of finer break. The "autosuspension model" used is shown in Fig. 25[23].

When a unit volume of sediments suspended in two-dimensional flows of turbidity currents are transported with the velocity u over the slope with an angle β, the sediments will be forced to move downwards by the power of $(\rho_s-\rho_\theta)gu\cdot\sin\beta$, and then the turbulence upward with the same power will occur on the basis of the law of conservation of energy. The upward turbulence is considered to prevent the suspended sediments from deposition.

In case of turbidity currents of a thickness h, the energy blance equations are represented by eqs. (9), (10) and (11).

$$(\rho_s-\rho_\theta)\, g\bar{C}huI-(\rho_s-\rho_\theta)\, gh\cdot K \geq \tau_0 u_1+\tau_i u_2 \tag{9}$$

$$\simeq (\tau_0+\tau_i)\, u \tag{10}$$

$$K=\sum \bar{C}_i w_i \tag{11}$$

$\bar{C}$: mean volume concentration ($=C_m\times 10^{-6}/\rho_s$, C_m: mean concentration of flowing water (mg/l)), $\bar{C}_i$, w_i: mean volume concentration and settling velocity (cm/s) respectively of sediment with a median diameter for each grain-size fraction, τ_0, τ_i, shear stress (g/cm/s^2) at bottom and interface calculated by ${u_{*b}}^2/\rho_1$ and ${u_{*a}}^2/\rho_2$, respectively (u_{*a}: friction velocity at interface (cm/s), ρ_2: bulk density of flowing water from maximum-velocity point to interface (g/cm^3)), u_1, u_2: mean velocity within the section from bottom to maximum-velocity point and from maximum-velocity point to interface, respectively (cm/s)

The first term on the left side of eq. (9) is all the power of turbulence per unit time produced by the "compelled settling" of sediment and the second term, the power expended by the fluid in lifting sediment, and the right side of eq. (9), the power spended owing to friction at bottom and interface.

Eqs. (9), (10) and (11) are made up for sediment mixtures, and the inequality in eq. (9), i.e. positive real numbers of K in eq. (11) can lead to the existence of sediment transported by the means of autosuspension.

Table 6 indicates the values of parameters substituted into eq. (9) and the results of K. The values of K for Points 3 and 5 are both positive, which show the being of sediment transported in a mode of autosuspension. On the other hand, the product of $\bar{C}_i$ and w_i was calculated and then summed in turn for each of the grain-size fractions ranging from finest to coarser. w_i was

Table 6 Values of parameters substituted into eq. (9) and the results of K for Points 3 and 5 in Run 10.

Run 10

Point No.	I	$\bar{C}$ (10^{-3})	h (cm)	u_1 (cm/s)	u_2 (cm/s)	τ_0 (g/cm/s^2)	τ_i (g/cm/s^2)	K $\times 10^{-6}$(cm/s)
3	0.010	3.58	9.14	6.78	6.52	0.286	0.233	5.53
5	0.010	3.07	8.95	6.12	5.88	0.302	0.134	4.20

computed by the Stokes equation, $(1/18)\{(\rho_s-\rho_\theta)/\mu\}\cdot gd^2$ (μ: viscosity (g/cm/s)), and $\bar{C}_i$, by the value of $\bar{C}$ in Table 6 and the grain-size distributions in Fig. 18.

As the result, $\sum\bar{C}_i w_i$ equal to the results of K in Table 6 almost conform to the values of summations for the suspended sediments finer than those with a grain size corresponding to finer break, and thus it is seen that the point of finer break is critical point distinguishing between suspension and autosuspension populations, and the autosuspension population of bottom sediments resulted from the same population of suspended sediments being deposited almost in an equilibrium with its transportation by flow (Figs. 15 and 17).

4. Application of experimental results to the field study

4.1 A fundamental viewpoint of application

Fig. 26 indicates the results of grain-size analysis for the bottom sediments of Katsurazawa Reservoir, sampled at each section on the fourth survey for October 27–29, 1976. The sediments at Nos. 1-A and 2 were sampled at the deepest points on sounding line, and those at No. 2-A, to the left 33 m distant from the old channel (see Fig. 3 in the previous paper[7]). The sampling point at No. 3 is shown in Fig. 27. A dotted line in Fig. 26 is the grain-size-distribution curve for suspended sediments in inflow water sampled at 7:54 on April 16, 1977 (Fig. 3), and described as comparison with the others.

Despite only one break of the cumulative curve for suspended sediments, the bottom sediments possess two or three breaks in log-probability plots which are common to the sediments in laboratory flume. Therefore, from a viewpoint of grain-size-distribution curves on log-probability paper for the bottom sediments, the experimental results can be applied to those of survey in Katsurazawa Reservoir.

On account of the close relationship between hydrodynamic characteristics of turbidity currents and grain-size distribution of bottom sediments, hydrological conditions should be given for turbidity currents *in situ*, flowing

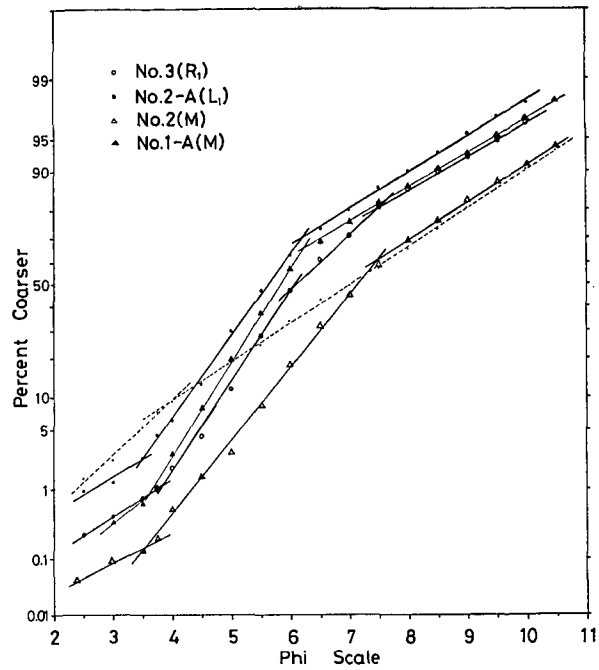

Fig. 26 Grain-size distributions of the bottom sediments of Katsurazawa Reservoir, sampled at each section for October 27–29, 1976. A dotted line on paper is the grain-size-distribution curve for suspended sediment in river water obtained at 7:54 on April 16, 1977.

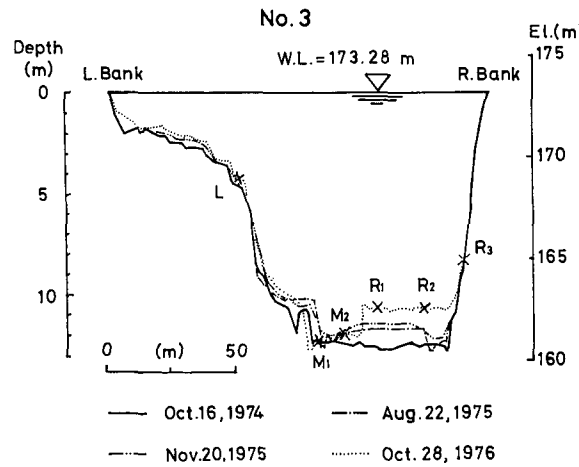

Fig. 27 Change in shape of the cross-sectional profiles and sediment-sampling points at the bottom of No. 3 section.

over each of the sediment-sampling points. On the basis of the observational results, hydrological conditions will be established first for the influent river and the reservoir, and then for turbidity currents.

4.2 Establishment of hydrological conditions of turbidity currents

Hydrological conditions of the Ikushunbetsu River and the reservoir can be first determined as follows:

In the year 1976 when the bottom sediments shown in Fig. 26 were sampled, there occurred few torrential runoffs before obtaining the sediments, and therefore most of the sediments will have been transported into the reservoir through sediment discharge of the Ikushunbetsu River during the period of spring thaw of 1976 (Fig. 28). Transport and deposition of the sediments in the reservoir would have been then performed actively by turbidity currents. As the result, the grain-size distributions of the sampled sediments will reflect both the hydrodynamic characteristics of turbidity currents and the grain-size distribution of suspended sediments, which will appear conspicuously at the time of the peak concentration of inflow water. During the snow-melting period of the year 1976, the peak concentration will have occurred sometime for the 14 day of April when the discharge recorded on the daily average reached the maximum.

Sediment discharge of the Ikushunbetsu River could not be measured for the snow-melting period of 1976, and however the daily-average discharge and the water level at 9:00 on April 14, 1976 are roughly equal to those on April

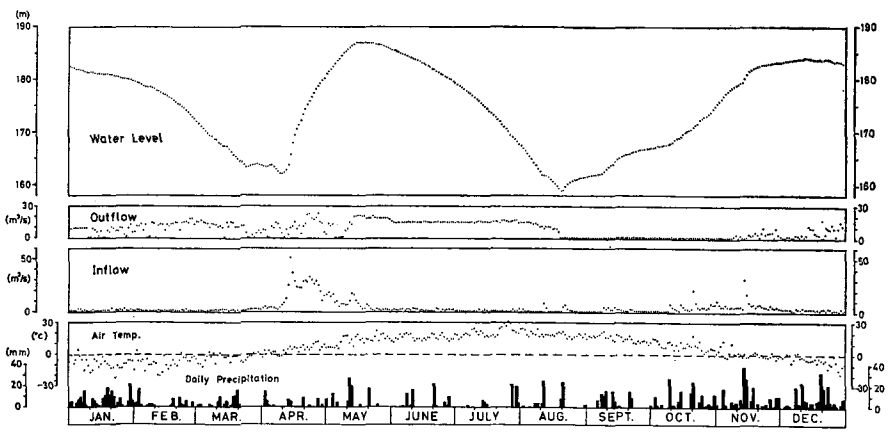

Fig. 28. Hydrological records of Katsurazawa Reservoir in the year 1976.

15, 1977, which are 51.52 m^3/s and 165.72 m, and 62.52 m^3/s and 165.51 m, respectively.

In the result, water concentration and discharge of the Ikushunbetsu River and water level of the reservoir at 14:56 on April 15, 1977 can be used as the maximums of concentration and discharge, and water level of the reservoir at the time of their occurrence for the 14th of April 1976, in consideration of the smaller daily-average discharge on the latter day. These were 9280 mg/l, 21.36 m^3/s and 164.67 m, respectively (Tables 1 and 3), which were lastly used as the hydrological conditions.

Subsequently, a hydrological condition of turbidity currents at each of the sediment-sampling points will be obtained.

When river water with the concentration of 9280 mg/l and the discharge of 21.36 m^3/s flows into the reservoir, plunging point, after the formation of mixing zone, can be located somewhere in the upstream reach of the reservoir, followed by occurrence of turbidity currents. The location of plunging point should be determined because of the change of a hydrological condition of turbidity currents at each of the sediment-sampling points, resulting from sedimentation while its flowing.

Fig. 29 indicates the experimental results on the relation of the densimetric Froude number Fr with the dimensionless parameter $\sqrt{sI}$ in mixing zone and turbidity currents. Mixing zone and turbidity currents can be distinguished by the number of subpopulations in log-probability plots of grain-size distributions of the bottom sediments (solid line). The line shows the relation between the two parameters at or near plunging point.

Egashira and Ashida[29] pointed out that h at plunging point is proportional chiefly to $q^{2/3}\cdot(sgI)^{-1/3}$, and therefore, based on the relation of $Fr=q/\sqrt{sgh^3}$ with $\sqrt{I}$, can be done the distinction between mixing zone and turbidity currents. However, in case of the results by the writer, the better distinction was obtained by the use of the relation between Fr and $\sqrt{sI}$[13]. The location of plunging point can be thus determined through trial-and-error method, from the solid line in Fig. 29 and the cross-sectional profile for each sediment-sampling point obtained by echo-sounding for October 27–29, 1976.

According to the results by Itakura and Kishi[13] and the writer, the entrainment coefficient at plunging point is 0.2, and so the discharge of 1.2 times 21.36 m^3/s and the concentration of inflow water were given to plunging point.

Water temperature was also considered to be the same as that of inflow

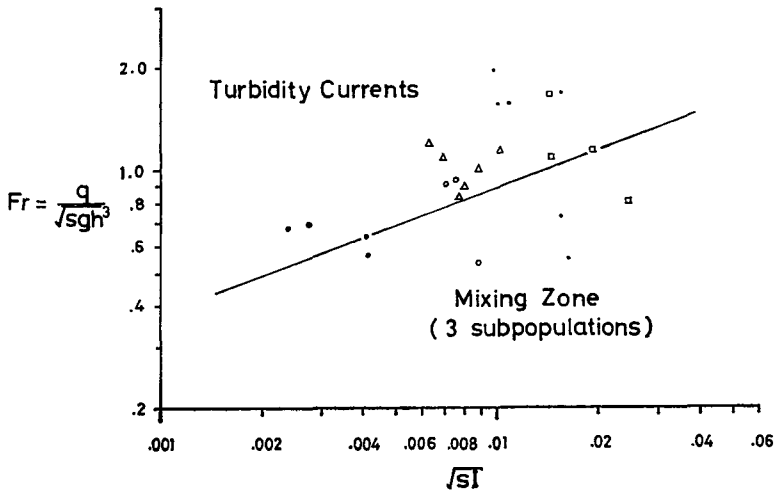

Fig. 29 Experimental results of the relation of Fr with $\sqrt{sI}$. (q: flow rate per unit width (cm²/s), $s=(\rho_{\theta c}-\rho_{\theta})/\rho_{\theta c}$, h: height from bottom to water surface in mixing zone and to interface in turbidity currents, I: bottom slope)

Table 7 Obtained results on location of plunging point.
April, 1977

Day	s	I	Fr	w.l. (m)	Q (m³/s)	h (cm)	Re (10^5)	Location of Plunging Point (Distance from Point No. 3)
15	0.00570	0.00587	0.729	164.67	25.63	182	2.73	150.2 m upstream
16	0.00652	0.00587	0.751	166.80	54.59	226	3.91	407.4 m upstream

water on the basis of the observational results in the field. Temperature and concentration of reservoir water were given by that of inflow water and 100 mg/l, respectively (Tables 3 and 8). Table 7 indicates the obtained results on location of plunging point, of which h is given as the hydraulic depth being the rate of the flow area to the width of water surface[30] and s is obtained from bulk density of flowing and reservoir waters at plunging point shown in Table 8. For the purpose of the comparison, shown are also the results for the data at 9:50 on April 16, 1977 (Table 1).

Lastly, a hydrological condition of turbidity currents at each sediment-sampling point will be determined in the following.

Table 8 indicates the conditions of turbidity currents and reservoir water at each point concerned with concentration and temperature.

Table 8 Conditions of turbidity currents and reservoir water at each point concerning concentration and temperature. In case of flowing water, C_m is a mean concentration of each cross section in a flow.

Flowing Water (April, 1977)

Day	15			16			
Point	C_m (mg/l)	θ (°C)	$\rho_{\theta c}$ (g/cm³)	C_m (mg/l)	θ (°C)	$\rho_{\theta c}$ (g/cm³)	
Plunging P.	9280	5.0	1.00578	10600	2.9	1.00661	
No. 3	8000	2.7	1.00498	9000	1.6	1.00557	$f_0=0.0535$
No. 2-A	5000	2.4	1.00310	6000	1.8	1.00371	
No. 2	2500	3.7	1.00156	4000	3.4	1.00249	$\alpha=0.558$
No. 1-A	2000	5.0	1.00124	2700	5.0	1.00168	

Reservior

Point	C_m (mg/l)	θ (°C)	$\rho_{\theta c}$ (g/cm³)
Plunging P.	100	5.0/2.9	1.00005
No. 3	100	0.3	0.99995
No. 2-A	100	2.0	1.00003
No. 2	600	5.0	1.00037
No. 1-A	1000	5.0	1.00062

Concentration of the turbidity currents was obtained in consideration of reservoir sediment distribution and a flowing distance downstream from located plunging point, and its water temperature was averaged by temperature of the reservoir water at the depth of a given sediment-sampling point and that of the turbidity currents at a sampling point upstream next to the given point. Concerning concentration and temperature of the reservoir water, used were the average values corresponding to those at the depth of each point obtained by the survey of reservoir water on April 29, 1977 and on March 29, 1978 (Table 2).

f_0 is the bottom friction factor and here defined by eq. (12).

$$f_0 = 8(\rho_{\theta c}-\rho_\theta)/\rho_{\theta c}\cdot I\cdot h/(1+\alpha)/u_m{}^2 \qquad (12)$$

$\rho_{\theta c}$, ρ_θ: bulk density of turbidity currents and reservoir water respectively, α: ratio of the height from maximum-velocity point to interface to that from bottom to maximum-velocity point, u_m: mean velocity of the cross section for each point (cm/s)

Fig. 30 indicates the relation of f_0 with the two dimensionless parameters Fr and I. This is based on the experimental data (mark x) by Ashida and

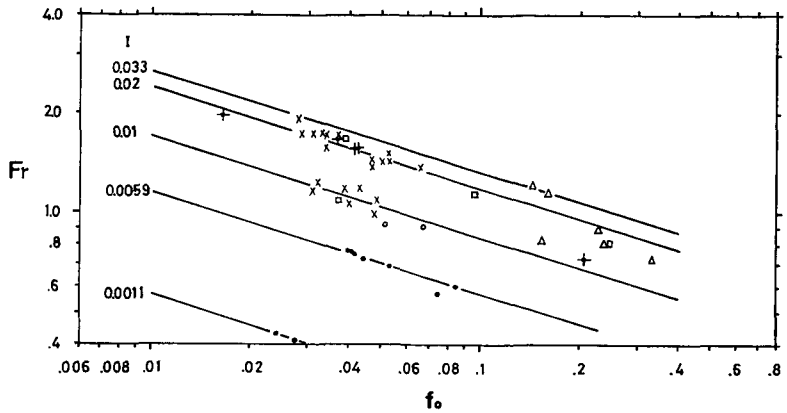

Fig. 30 Relation of f_0 with Fr and I on the basis of experimental and observational data. The mark × represents the results by Ashida and Egashira[12]. (○: Run 10, +: Run 12, △: Run 15, □: Run 18)

Egashira[12], and the experimental and observational data by the writer. The plots to $I=0.0011$ and 0.0059 were obtained through calculation of f_0 at plunging point *in situ* by the use of the observational data on sediment discharge in April 1977, from the fact that the profile of vertical distribution of flow velocity at plunging point is symmetrical, i.e. $\alpha=1$ in eq. (12)[13].

In the result, f_0 for turbidity currents at each point was given constant 0.0535 by Fig. 30 and the mean bed slope I at each point, in consideration of a limited range of the values of Fr for all the sampling points.

Since α in eq. (12) was seen to be independent of Fr and Re on flow and the other main parameters through the experiments by Ashida and Egashira[12], and the writer, its average value 0.558 was given.

Table 9 indicates the obtained results of the main parameters for turbidity currents flowing over each point. This was given by trial-and-error method through substitution of the values in Table 8 and the known parameter Q into eqs. (12) and (13) and the availability of the cross-sectional profile on each point obtained by echo-sounding for October 27–29, 1976. Eq. (13) is a equation of continuity and applied to the flows crossing each section.

$$Q = u_m \cdot A \qquad (= \text{const.}) \tag{13}$$

A: cross-sectional area of the turbidity currents at each section

Table 9 Obtained results of the main parameters on turbidity currents flowing over each sediment-sampling point.

Apr. 15, 1977

Point No.	I	s	h (cm)	u_m (cm/s)	Fr	Re (10^5)
3	0.00349	0.00501	177	16.5	0.563	1.87
2-A	0.00539	0.00306	109	11.6	0.637	0.813
2	0.00488	0.00119	222	12.8	0.698	1.83
1-A	0.00464	0.00062	273	12.2	0.668	2.15

Apr. 16, 1977

Point No.	I	s	h (cm)	u_m (cm/s)	Fr	Re (10^5)
3	0.00349	0.00559	269	21.6	0.562	3.60
2-A	0.00539	0.00367	151	17.2	0.733	1.61
2	0.00488	0.00212	296	18.5	0.688	3.42
1-A	0.00464	0.00106	320	15.3	0.666	3.05

4.3 Results of application

By the use of the results in Tables 8 and 9, the bottom friction velocity u_{*b} for turbidity currents at each point was obtained by eq. (14).

$$u_{*b} = \{(\rho_{\theta c}-\rho_\theta)/\rho_{\theta c}\cdot g\cdot I\cdot h/(1+\alpha)\}^{1/2} \tag{14}$$

The Reynolds number Re on particle can be thus given by eq. (6) for each break point in log-probability plots shown in Fig. 26, and then its relation with Fr was checked up.

Fig. 31 indicates the relation of Fr with Re for the break at about 3.5ϕ in Fig. 26. The black and white plots show the results under date of April 15 and 16, 1977 respectively. The solid line on paper is obtained by the experimental result by the writer (Fig. 20). The blacks are evidently representative of a better agreement with the experimental result for coarser break, and therefore the break in question is seen to be "coarser break" being truncation between traction and saltation populations.

Fig. 32 indicates the relation of Fr with Re for the break positioned at the phi value of 7.40 for the No. 2 sediments and at about 6.0ϕ for the others. The black plots showing the results under date of April 15 are likewise in better agreement with the experimental one (solid line) for middle break. This means that the break in question is "middle break" equivalent to truncation between saltation and suspension populations.

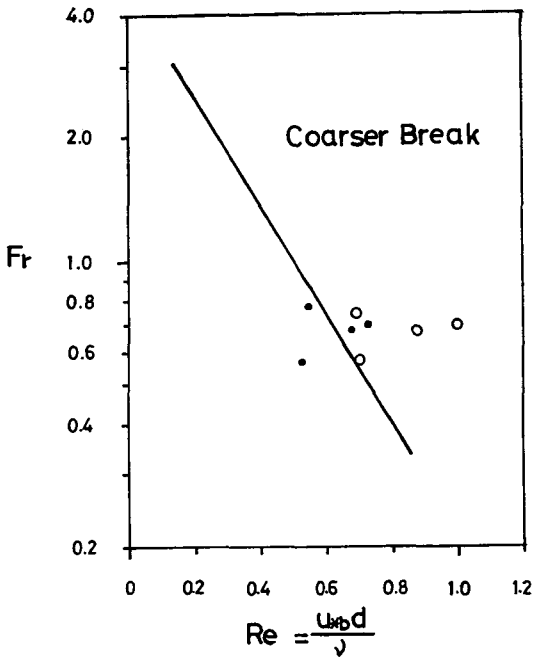

Fig. 31 Relation of Fr with Re for the break correspondent to about 3.5 in phi scale in Fig. 26.

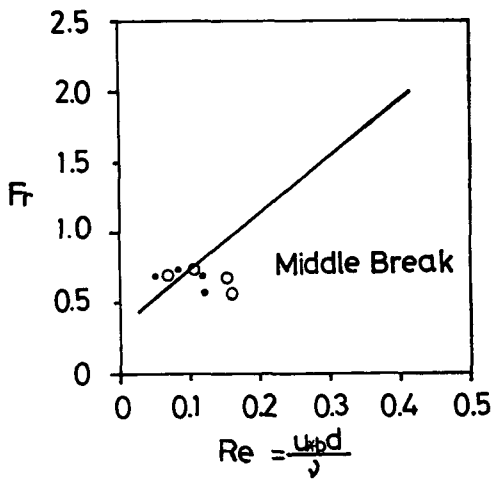

Fig. 32 Relation of Fr with Re for the break positioned at the phi value of 7.40 or about 6.0 in Fig. 26.

With respect to another break for the No. 3 sediments, occurring at 7.47ϕ, the plots are shown in Fig. 23 (two bigger circles). In this case, conversely, the result under date of April 16 show a better conformity to the experimental one. However, this can be rather considered to be indicative of no correlation between Fr and Re, and therefore whether the break under consideration is the so-called "finer break" should be ascertained by the use of eqs. (10) and (11).

Table 10 indicates the parameters on turbidity currents substituted into eq. (10) and the calculational result of K at each point.

Table 10 Values of the parameters on turbidity currents substituted into eq. (10) and the calculational result of K at each point.

Point No.	I	$\bar{C}$ (10^{-3})	h (cm)	u_{m} (cm/s)	τ_0 (g/cm/s^2)	τ_i	K $\times 10^{-7}$(cm/s)
3	0.00349	3.01	177	16.5	1.884	1.134	5 57
2-A	0.00539	1.87	109	11.6	1.121	0.674	−3.92
2	0.00488	0.930	222	12.8	1.032	0.621	−4.38
1-A	0.00464	0.750	273	12.2	0.966	0.582	−2.70

K is negative except for Point No. 3, which shows no transport and deposition of the suspended sediments in a mode of autosuspension at the points other than Point No. 3. Since the sediments autosuspended in flow at Point No. 3 were considered to be little deposited on the bed from the inlet of the Ikushunbetsu River to Point No. 3, $\bar{C}_i w_i$ was integrated for finest to coarser grain-size fractions, from grain-size distribution of the sediments suspended in river water and its concentration (Table 1 and Fig. 3).

As the result, the largest value of the settling velocity w_i in the obtained $\sum \bar{C}_i w_i$ was almost equal to that for a grain size correspondent to the break in question, and therefore the break can be considered to be "finer break" being truncation between suspension and autosuspension populations.

The reservoir sediments on the beds near plunging point can be thus divided into the four subpopulations, i.e. traction, saltation, suspension and autosuspension populations. This can be caused by the higher concentration of flowing water in turbidity currents near plunging point.

Fig. 33 indicates the division of populations by different modes in transport and deposition of the reservoir sediments shown in Fig. 26.

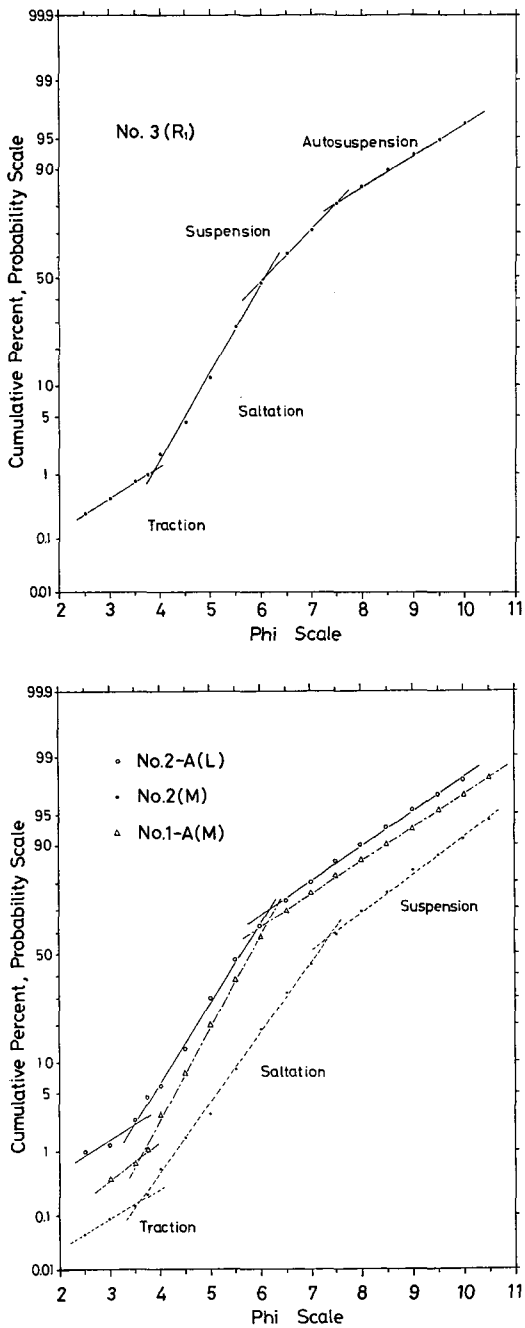

Fig. 33 Division of populations by different modes in transprot and deposition of the reservoir sediments shown in Fig. 26.

5. Conclusions

(1) Observations were made on sediment discharge of the rivers flowing into the reservoir for April 3–29, 1977 and March 29, 1978 in order to ascertain the fact that turbidity currents can occur during the snow-melting period every year.

The observed peak concentration of waters of the Ikushunbetsu River reached 11,900 mg/l during the surveying period, and the sediment concentrations more than 10,000 mg/l lasted about 18 hours from April 15 to 16. On the other hand, the bottom layer of the reservoir turned so turbid as snow melting progressed. It was thus shown that actually turbidity currents can occur during the period of spring thaw and can be divided into three types of overflows, interflows and underflows considering little effects of temperature difference on density difference between river water and reservoir water, and its period has an adequate condition to induce such turbidity currents as underflows.

(2) Sedimentation by turbidity currents was investigated more elaborately by laboratory experiment with a flume. Taking notice of break points in log-probability plots of grain-size distributions of the bottom sediments in a flume, the division of the sediments into a few subpopulations was attempted through casting light on sedimentological implications of the break points.

As the result, the sediments in mixing zone and/or in turbidity currents near plunging point can be divided into three subpopulations, i.e. traction, saltation and suspension populations, and those in turbidity currents, into four subpopulations, namely traction, saltation, suspension and autosuspension populations.

(3) From the fact that the bottom sediments of Katsurazawa Reservoir possess a few breaks in log-probability plots of grain-size distributions, the experimental results were applied for the purpose of an interpretation of the mode in transport and deposition of the reservoir sediments.

As the result, the calculational results for turbidity currents *in situ* on the basis of the observational and experimental data represented a good agreement with the experimental ones.

It was thus shown that through sedimentation by turbidity currents, the reservoir sediments on the bed near plunging point can be divided into the four subpopulations, namely traction, saltation, suspension and autosuspension populations, and the sediments far downstream from there, into the three subpopulations, i.e. traction, saltation and suspension populations.

Acknowledgements: The writer wishes to express grateful thanks to Professor K. Nakao of Hokkaido University for valuable discussions and constant encouragement during the course of this study. Appreciation is due to the members of the Control Office of Katsurazawa Reservoir for their cooperation in performing the observations of the reservoir and analyzing the data. The writer is also indebted to Mr. K. Yamaguchi for his help in the design and construction of the experimental apparatus, and Messrs. H. Izuta and E. Emoto and the other members of Lecture on Hydrology, Department of Geophysics for their assistance in carrying out the experiment.

This paper was submitted to Hokkaido University in July 1979 as the writer's doctorial thesis.

References

1) KUENEN, Ph. H. and MIGLIORINI, C.I.: Turbidity currents as a cause of graded bedding. J. Geol., **58**, (1950), 91–127.
2) KUENEN, Ph. H. and MENARD, H.W.: Turbidity currents, graded and non-graded deposits. J. Sed. Petrol., **22**, (1952), 83–96.
3) SANDERS, J.E.: Concepts of fluid mechanics provided by primary sedimentary structures. J. Sed. Petrol., **33**, (1963), 173–179.
4) SANDERS, J.E.: Primary sedimentary structures formed by turbidity currents and related resedimentation mechanisms. In G.V. MIDDLETON (ed.), Primary Sedimentary Structures and their Hydrodynamic Interpretation. Soc. Econ. Paleontologists and Mineralogists, Spec. Pub. No. **12**, (1965), 192–219.
5) KUENEN, Ph. H.: Experimental turbidite lamination in a circular flume. J. Geol., **74**, (1966), 523–545.
6) KUENEN, Ph. H.: Emplacement of flysch-type sand beds. Sedimentology, **9**, (1967), 203–243.
7) CHIKITA, K.: Sedimentation by turbidity currents – Katsurazawa Reservoir. –. Jap. J. Limnol., **38**, (1977), 48–61 (in Japanese).
8) KUENEN, Ph. H.: Estimated size of the Grand Banks turbidity current. Amer. J. Science, **250**, (1952), 874–884.
9) MIDDLETON, G.V.: Experiments on density and turbidity currents. II. Uniform flow of density currents. Can. J. Earth Sci., **3**, (1966), 627–637.
10) STEFAN, H.: High concentration turbidity currents in reservoirs. Proc. 15th Con. of IAHR, **1**, (1973), A44–1–A44–12.
11) ASHIDA, K. and EGASHIRA, S.: Condition of occurrence of turbidity currents. Proc. the 29th Ann. Confer. Japan Soc. Civil Eng., II, (1974), 439–440 (in Japanese).
12) ASHIDA, K. and EGASHIRA, S.: Basic study on turbidity currents. Trans. Japan Soc. Civil Eng., No. **237**, (1975), 37–50 (in Japanese).
13) ITAKURA, T. and KISHI, T.: Study on reservoir density currents. Proc. the 14th Synth. Sympo. Sci. Natural Disas., (1977), 89–91 (in Japanese).
14) SMITH, W.O. et al.: Comprehensive survey of sedimentation in Lake Mead, 1948–49. Geol. Surv. Prof. Paper, **295**, (1960), 254 pp.
15) HEEZEN, B.C. and EWING, M.: Turbidity currents and submarine slumps, and the

1929 Grand Banks earthquake. Amer. J. Science, **250**, (1952), 849–873.
16) GOULD, H.R.: Turbidity currents. In W.O. SMITH et al., Comprehensive Survey of Sedimentation in Lake Mead, 1948–49. Geol. Surv. Prof. Paper, **295**, (1960), 201–207.
17) HJULSTRÖM, F.: Studies of the morphological activity of rivers as illustrated by the River Fyris. Bull. Geol. Inst. Uppsala, **25**, (1935), 221–257.
18) KIKKAWA, H.: A few considerations of transport rate of suspended sediments. Rep. Inst. Civ. Eng., **83**, (1952), 25–37 (in Japanese).
19) LOFQUIST, K.: Flow and stress near an interface between stratified liquids. The Phy. of Fluids, **3**, (1960), 158–175.
20) VISHER, G.S.: Grain size distributions and depositional processes. J. Sed. Petrol., **39**, (1969), 1074–1106.
21) VISHER, G.S.: Physical characteristics of fluvial deposits. In J.H. RIGBY and W.K. HAMBLIN (ed.), Recognition of Ancient Sedimentary Environments. Soc. Econ. Paleontologists and Mineralogists, Spec. Pub., No. **16**, (1972), 84–97.
22) SAGOE, K.O. and VISHER, G.S.: Population breaks in grain-size distributions of sand-a theoretical model. J. Sed. Petrol., **47**, (1977), 285–310.
23) BAGNOLD, R.A.: Auto-suspension of transported sediment; turbidity currents. Proc. Roy. Soc. London, Ser. A, **265**, (1962), 315–319.
24) INMAN, D.L.: Measures for describing the size distribution of sediments. J. Sed. Petrol., **22**, (1952), 125–145.
25) YALIN, M.S.: Mechanics of sediment transport. (1972), 290pp, Pergamon Press.
26) SUNDBORG, Å.: The river Klarälven, a study of fluvial processes. Geogr. Ann., **38**, (1956), 127–316.
27) FRANCIS, J.R.D.: Experiments on the motion of solitary grains along the bed of a water-stream. Proc. Roy. Soc. London, Ser. A, **332**, (1973), 443–471.
28) BAGNOLD, R.A.: The nature of saltation and of 'bed load' transport in water. Proc. Roy. Soc. London, Ser. A, **332**, (1973), 473–504.
29) EGASHIRA, S. and ASHIDA, K.: Inference of water depth of plunging point on reservoir density currents. Proc. the 15th Synth. Sympo. Sci. Natural Disas., (1978), 481–482 (in Japanese).
30) CHOW, V.T.: Open-channel hydraulics. (1959), 680pp, McGraw-Hill.